Interfaces detection after corneal refractive surgery by low coherence optical interferometry

I. Verrier,[1,2,*] C. Veillas,[1,2] T. Lépine,[1,2,4] F. Nguyen,[1,3] G. Thuret,[1,3] and P. Gain[1,3]

[1]*Université de Lyon, F-42023, Saint-Etienne, France*
[2]*CNRS, UMR 5516, Laboratoire Hubert Curien, F-42000 Saint-Etienne, France;*
[3]*Laboratoire Biologie, Ingénerie et Imagerie de la Greffe de Cornée, JE2521, IFR143, Université Saint-Etienne, Jean Monnet, F-42000, Saint-Etienne, France*
[4]*Institut d'Optique Rhône-Alpes, 18, rue Benoît LAURAS 42000 Saint-Etienne, France*
**isabelle.verrier@univ-st-etienne.fr*

Abstract: The detection of refractive corneal surgery by LASIK, during the storage of corneas in Eye Banks will become a challenge when the numerous operated patients will arrive at the age of cornea donation. The subtle changes of corneal structure and refraction are highly suspected to negatively influence clinical results in recipients of such corneas. In order to detect LASIK cornea interfaces we developed a low coherence interferometry technique using a broadband continuum source. Real time signal recording, without moving any optical elements and without need of a Fourier Transform operation, combined with good measurement resolution is the main asset of this interferometer. The associated numerical processing is based on a method initially used in astronomy and offers an optimal correlation signal without the necessity to image the whole cornea that is time consuming. The detection of corneal interfaces - both outer and inner surface and the buried interface corresponding to the surgical wound – is then achieved directly by the innovative combination of interferometry and this original numerical process.

OCIS codes: (120.0120) Instrumentation, measurement and metrology; (120.3180) Interferometry; (170.4470) Ophthalmology; (170.4500) Optical coherence tomography; (330.7327) Visual optics, ophthalmic instrumentation; (330.7335) Visual optics, refractive surgery.

References and links

1. I. G. Pallikaris, M. E. Papatzanaki, D. S. Siganos, and M. K. Tsilimbaris, "A corneal flap technique for laser in situ keratomileusis. Human studies," Arch. Ophthalmol. **109**(12), 1699–1702 (1991).
2. H. P. Sandoval, L. E. de Castro, D. T. Vroman, and K. D. Solomon, "Refractive Surgery Survey 2004," J. Cataract Refract. Surg. **31**(1), 221–233 (2005).
3. M. Vesaluoma, J. Pérez-Santonja, W. M. Petroll, T. Linna, J. Alió, and T. Tervo, "Corneal stromal changes induced by myopic LASIK," Invest. Ophthalmol. Vis. Sci. **41**(2), 369–376 (2000).
4. G. D. Kymionis, N. Tsiklis, A. I. Pallikaris, V. Diakonis, G. Hatzithanasis, D. Kavroulaki, M. Jankov, and I. G. Pallikaris, "Long-term results of superficial laser in situ keratomileusis after ultrathin flap creation," J. Cataract Refract. Surg. **32**(8), 1276–1280 (2006).
5. G. D. Kymionis, N. Tsiklis, A. I. Pallikaris, D. I. Bouzoukis, and I. G. Pallikaris, "Fifteen-year follow-up after LASIK: case report," J. Refract. Surg. **23**(9), 937–940 (2007).
6. M. J. Maldonado, L. Ruiz-Oblitas, J. M. Munuera, D. Aliseda, A. García-Layana, and J. Moreno-Montañés, "Optical coherence tomography evaluation of the corneal cap and stromal bed features after laser in situ keratomileusis for high myopia and astigmatism," Ophthalmology **107**(1), 81–87, discussion 88 (2000).
7. R. J. Farias, A. Parolim, and L. B. Sousa, "[Corneal transplant utilizing a corneal graft that had undergone laser surgery--case report]," Arq. Bras. Oftalmol. **68**(2), 266–269 (2005).
8. A. Michaeli-Cohen, A. C. Lambert, F. Coloma, and D. S. Rootman, "Two cases of a penetrating keratoplasty with tissue from a donor who had undergone LASIK surgery," Cornea **21**(1), 111–113 (2002).
9. S. Langner, H. Martin, T. Terwee, S. A. Koopmans, P. C. Krüger, N. Hosten, K. P. Schmitz, R. F. Guthoff, and O. Stachs, "7.1T MRI to Assess the Anterior Segment of the Eye," Invest. Ophthalmol. Vis. Sci. **4**, (2010), doi:10.1167/iovs.09-4865.
10. Y. Zeng, Y. Liu, X. Liu, C. Chen, Y. Xia, M. Lu, and M. He, "Comparison of lens thickness measurements using the anterior segment optical coherence tomography and A-scan ultrasonography," Invest. Ophthalmol. Vis. Sci. **50**(1), 290–294 (2009).

#135460 - $15.00 USD Received 21 Sep 2010; revised 10 Nov 2010; accepted 12 Nov 2010; published 19 Nov 2010

11. P. Rosales, A. de Castro, I. Jiménez-Alfaro, and S. Marcos, "Intraocular lens alignment from Purkinje and Scheimpflug imaging," Clin. Exp. Optom. **93**(6), 400–408 (2010), doi:10.1111/j.1444-0938.2010.00514.x.
12. C. Wirbelauer, H. Aurich, and D. T. Pham, "Online optical coherence pachymetry to evaluate intraoperative ablation parameters in LASIK," Graefes Arch. Clin. Exp. Ophthalmol. **245**(6), 775–781 (2007).
13. M. J. Doughty, and M. L. Zaman, "Human corneal thickness and its impact on intraocular pressure measures: a review and meta-analysis approach," Surv. Ophthalmol. **44**(5), 367–408 (2000).
14. S. G. Priglinger, A. S. Neubauer, C. A. May, C. S. Alge, A. H. Wolf, A. Mueller, K. Ludwig, A. Kampik, and U. Welge-Luessen, "Optical coherence tomography for the detection of laser in situ keratomileusis in donor corneas," Cornea **22**(1), 46–50 (2003).
15. A. H. Wolf, A. S. Neubauer, S. G. Priglinger, A. Kampik, and U. C. Welge-Luessen, "Detection of laser in situ keratomileusis in a postmortem eye using optical coherence tomography," J. Cataract Refract. Surg. **30**(2), 491–495 (2004).
16. A. S. Neubauer, S. G. Priglinger, M. J. Thiel, C. A. May, and U. C. Welge-Lüssen, "Sterile structural imaging of donor cornea by optical coherence tomography," Cornea **21**(5), 490–494 (2002).
17. R. C. Lin, Y. Li, M. Tang, M. McLain, A. M. Rollins, J. A. Izatt, and D. Huang, "Screening for previous refractive surgery in eye bank corneas by using optical coherence tomography," Cornea **26**(5), 594–599 (2007).
18. G. Latour, G. Georges, L. S. Lamoine, C. Deumié, J. Conrath, and L. Hoffart, "Human graft cornea and laser incisions imaging with micrometer scale resolution full-field optical coherence tomography," J. Biomed. Opt. **15**(5), 056006 (2010).
19. W. Y. Oh, B. E. Bouma, N. Iftimia, S. H. Yun, R. Yelin, and G. J. Tearney, "Ultrahigh-resolution full-field optical coherence microscopy using InGaAs camera," Opt. Express **14**(2), 726–735 (2006).
20. B. Povazay, K. Bizheva, A. Unterhuber, B. Hermann, H. Sattmann, A. F. Fercher, W. Drexler, A. Apolonski, W. J. Wadsworth, J. C. Knight, P. S. Russell, M. Vetterlein, and E. Scherzer, "Submicrometer axial resolution optical coherence tomography," Opt. Lett. **27**(20), 1800–1802 (2002).
21. N. A. Nassif, B. Cense, B. H. Park, M. C. Pierce, S. H. Yun, B. E. Bouma, G. J. Tearney, T. C. Chen, and J. F. de Boer, "In vivo high-resolution video-rate spectral-domain optical coherence tomography of the human retina and optic nerve," Opt. Express **12**(3), 367–376 (2004).
22. J. M. Schmitt, "Optical Coherence Tomography (OCT): A review," IEEE J. Sel. Top. Quantum Electron. **5**(4), 1205–1215 (1999).
23. B. E. Bouma, and G. J. Tearney, *Handbook of optical coherence tomography*, (New York: Marcel Dekker, 2002).
24. R. Leitgeb, M. Wojtkowski, A. Kowalczyk, C. K. Hitzenberger, M. Sticker, and A. F. Fercher, "Spectral measurement of absorption by spectroscopic frequency-domain optical coherence tomography," Opt. Lett. **25**(11), 820–822 (2000).
25. Y. Park, T. J. Ahn, J. C. Kieffer, and J. Azaña, "Optical frequency domain reflectometry based on real-time Fourier transformation," Opt. Express **15**(8), 4597–4616 (2007).
26. K. Ben Houcine, M. Jacquot, I. Verrier, G. Brun, and C. Veillas, "Imaging through a scattering medium with an interferential spectrometer by selection of an amplitude modulation correlator," Opt. Lett. **29**(24), 2908–2910 (2004).
27. I. Verrier, C. Veillas, and T. Lépine, "Low coherence interferometry for central thickness measurement of rigid and soft contact lenses," Opt. Express **17**(11), 9157–9170 (2009).
28. V. Tombelaine, C. Lesvigne, P. Leproux, L. Grossard, V. Couderc, J. L. Auguste, J. M. Blondy, G. Huss, and P. H. Pioger, "Ultra wide band supercontinuum generation in air-silica holey fibers by SHG-induced modulation instabilities," Opt. Express **13**(19), 7399–7404 (2005).
29. I. Verrier, G. Brun, and J. P. Goure, "SISAM interferometer for distance measurements," Appl. Opt. **36**(25), 6225–6230 (1997).
30. L. Froehly, and R. Leitgeb, "Scan-free optical correlations techniques: history and applications to optical coherence tomography," J. Opt. **12**(8), 084001 (2010), doi:10.1088/2040-8978/12/8/084001.
31. Y. Watanabe, K. Yamada, and M. Sato, "Three-dimensional imaging by ultrahigh-speed axial-lateral parallel time domain optical coherence tomography," Opt. Express **14**(12), 5201–5209 (2006).
32. D. G. Dawson, I. Schmack, G. P. Holley, G. O. Waring 3rd, H. E. Grossniklaus, and H. F. Edelhauser, "Interface fluid syndrome in human eye bank corneas after LASIK: causes and pathogenesis," Ophthalmology **114**(10), 1848–1859 (2007).

1. Introduction

Refractive corneal surgery is one of the most frequent surgical act worldwide. Among surgical techniques available, LASIK [1] is widespread since more than 15 years and concerns millions of young patients, most of the time treated in both eyes [2]. It consists of the creation of an anterior flap of 9 to 10 mm diameter, within the anterior corneal stroma (80 to 170 micrometers in depth, on 300°), using either a surgical blade or a femtosecond laser. The cutting plan is parallel to corneal surface. The flap is then temporarily reclined and a customized volume of corneal tissue is vaporized by photoablation using an excimer laser, according to the preoperative ametropia and the expected refractive power. At the end of the process, the anterior flap is repositioned and corneal wound healing is effective after a few

#135460 - $15.00 USD Received 21 Sep 2010; revised 10 Nov 2010; accepted 12 Nov 2010; published 19 Nov 2010

days or weeks. Postoperatively, the intrastromal interface, as well as the circular cutting edges, become rapidly practically invisible with routine ophthalmological slit lamp. Nevertheless it remains detectable during years, using anterior segment optical coherent tomography (OCT) with commercial devices or confocal microscopy [3–6].

During all the process of corneal graft, from donation to graft into the recipient, the quality of the tissue is highly monitored. A drastic selection process eliminates nearly 50% of retrieved corneas, in order to deliver only very good quality grafts. The subtle alterations of stromal structure, thickness and optical properties, induced by refractive surgery, are highly suspected to influence postoperative issue of corneal graft, with an increased risk of refractive error. A risk for intraoperative flap dislocation has also been reported, as well as an epithelial downgrowth at the interface [7,8]. Efforts are therefore necessary to screen donors for history of refractive surgery.

Up to know, regarding the today mean donor age, and the relatively recent history of refractive surgery, patient having had a LASIK remains scarce. Nevertheless, the proportion of such donors will mathematically dramatically increase in a near future and become a daily preoccupation in Eye banks. Up to now, among techniques used in anterior segment imaging (MRI [9], USG [10], Scheimplung and Purkinje imaging [11]), there are no validated methods to screen corneas for refractive surgery. The slit lamp examination of cornea is not sensitive enough because of the post mortem corneal changes (epithelial desiccation or edema, stromal edema, posterior folds due to eye ball hypotony). Moreover, this method of examination is possible only in countries where eyeball enucleation is authorized after cornea donation (because it requires to place the intact eyeball in front of the slit lamp) and is virtually impossible when corneas are retrieved by in situ excision (only corneas with a thin rim of sclera are retrieved) and immediately immersed in a storage medium. Most of the time, the fine observation of the cornea immersed in a medium colored with red phenol (a pH indicator necessary to reveal microbiological contaminations) is impossible and makes unlikely the detection of the interfaces. It must be noted that retrieval by in situ excision concerns nearly half of the retrieval worldwide. The simple measurement of corneal thickness is also useless because the post mortem and storage induced edema almost doubles the total thickness (1000 micrometers) and hinders from detecting a 20 to 100 micrometers photoablation [12] in human corneas that physiologically vary around 536+/−31 micrometers [13]. The use of a commercial anterior segment OCT to assess the stored corneas have been reported [14–17]. This OCT seems to be able to detect interface in an in vitro model of LASIK for human corneas maintained up to 6 months in organ culture, as well as in real LASIK performed 15 months before death of one donor [14] or 9 months in another case [15]. More recently, a custom made table top OCT based on the same principle as commercial OCT, was able to detect changes in flap reflectivity but unable to visualize the interface in five LASIK corneas, possibly because of a longer post operative period [17].

OCT is an non-contact technique based on the use of a low coherence interferometer employing most of the time near infra-red light. OCT can acquire 3D images in few seconds. The principle of the measurement consists in comparing a reference light with the reflected light from the different layers of the cornea under test. To do that, in time domain OCT (TD-OCT), the delay line is moving to modulate the reference path (A-Scan corresponding to the sample depth) and the sample is scanned on its transverse directions (en face information). For example, a standard commercial OCT apparatus, using superluminescent diodes (SLED) at the wavelength of 1310 nm, authorizes a measurement with a precision of the order of 18 μm in depth. When using optical sources with wide spectral range, the axial resolution could reach 1 or 2 μm [18,19]. Submicrometer axial resolution has been achieved by use of a photonic crystal fiber in combination with a Ti:sapphire laser [20]. The spectral domain OCT (SD-OCT), which analyzes each frequency of the interfering signal by a spectrometer, is now also available in routine leading to a depth resolution of roughly 6 μm [21]. The drawback of the TD-OCT is that it is a time consuming method because it needs several acquisitions to analyze each depth position [22,23]. For SD-OCT, the main limitation is the sensitivity decay

#135460 - $15.00 USD Received 21 Sep 2010; revised 10 Nov 2010; accepted 12 Nov 2010; published 19 Nov 2010

with the measurement depth [24,25]. Moreover, the high cost of commercial devices hinders from diffusion to the community of Eye Banks.

Like other OCT, the method presented in this paper [26] is also based on low coherence interferometry and has been already applied to measurement of central thickness of contact lenses [27]. Our technique has been now adapted to be devoted to a very specific application, namely the interfaces detection of corneas after LASIK during corneal storage in Eye banks. Contrary to clinical application in vivo, image of the whole cornea as realized in classical OCT is not required for this application. Indeed, eye bankers and ophthalmologists need only to know whether corneas had a LASIK or not. Consequently, our experiment seems adapted because of the enhancement of the signal to noise ratio achieved by an original recording and numerical process and is similar to a direct A-scan without any moving elements. Experimental verification was performed on rabbit corneas after stromal dissection of a superficial flap.

The first part of this paper concerns a brief description of the set-up and of the expected signals for cut corneas. The second part presents the novel numerical processing allowing the increase of the signal to noise ratio. Finally, the last part is devoted to the experimental procedure concerning the rabbit corneas preparation and shows two measurements with significant results that demonstrate the ability of the system to detect in real time the buried interface of the cornea.

2. Measurement principle

2.1 Description of the set-up

The experimental set-up is nearly similar to the one described in reference [27]. The light of a supercontinuum source generated in an air-silica Microstructured Optical Fiber (MOF) pumped by a picoseconds microchip laser [28] is injected in a Mach-Zehnder interferometer, which is followed by a SISAM (Spectromètre Interférentiel à Sélection par l'Amplitude de Modulation) optical correlator (Fig. 1). In the Mach-Zehnder interferometer, the reference arm contains a delay line that is adjusted once at the beginning and that keeps the same position during the acquisition. The sample is set in the measurement arm at the focal point of a (10X) microscope objective leading to a theoretical transverse resolution of 3 μm (calculated at 700 nm). Because of the broadband spectrum of the source (spectral bandwidth of $\Delta\lambda_s$ = 1580 nm around the central wavelength λ_s = 1064 nm), a couple of similar objectives (10X) has been added in the reference arm in order to compensate the dispersion brought by the objective in the measurement arm. This change permits to improve the detection of the correlation peaks in comparison with the results obtained in the previous work [27]. Indeed, the peaks are thinner and the axial resolution is consequently increased (see §3.1). The SISAM is constituted of two diffraction gratings of N_0 = 150 lines number per millimeter, a beam-splitter, an imaging lens and a CCD video digital camera (Sony XCD-SX910 with 1280*960 pixels and a 15 fps maximum frame rate) with high sensitivity, large dynamic range and good resolution (10 bits). Moreover, this digital camera is more adapted in terms of gain control (from 0 to 24 dB) to the detection of the correlation peaks for the aimed application (cornea interfaces detection) than the analogical one (0-18 dB) used in [27]. The sensitivity range of the CCD (400 nm to 1000 nm) affects theoretically the axial resolution but in our case, is not the limiting factor (see §.3.1).

#135460 - $15.00 USD Received 21 Sep 2010; revised 10 Nov 2010; accepted 12 Nov 2010; published 19 Nov 2010

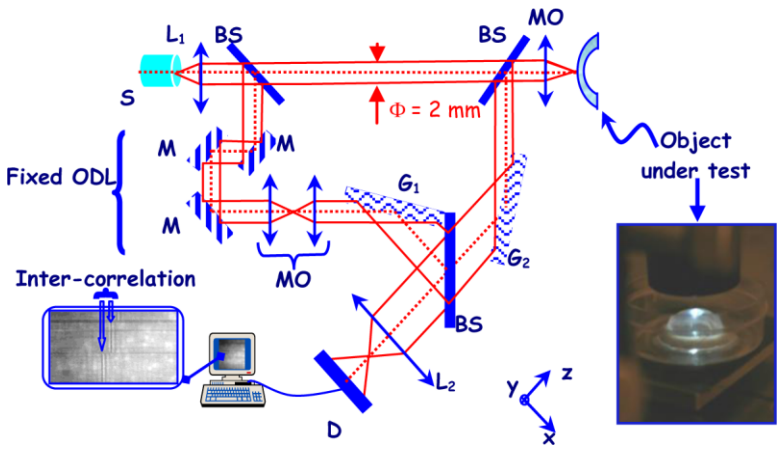

Fig. 1. Set-up. S: Source; $L_{1,2}$: Lenses; BS: Beam-splitter; MO: Microscope objective; M: Mirror; $G_{1,2}$: Gratings; ODL: Optical Delay Line; D: Detector.

2.2 Expression of the expected signal

In the reference arm, the wave propagates in air up to the first diffraction grating and remains nearly collimated. In the object arm, the wave propagates in air up to the 10x microscope objective, is focalized and reflected back by each interface of the sample leading to a set of echoes upon the second diffraction grating (Fig. 2).

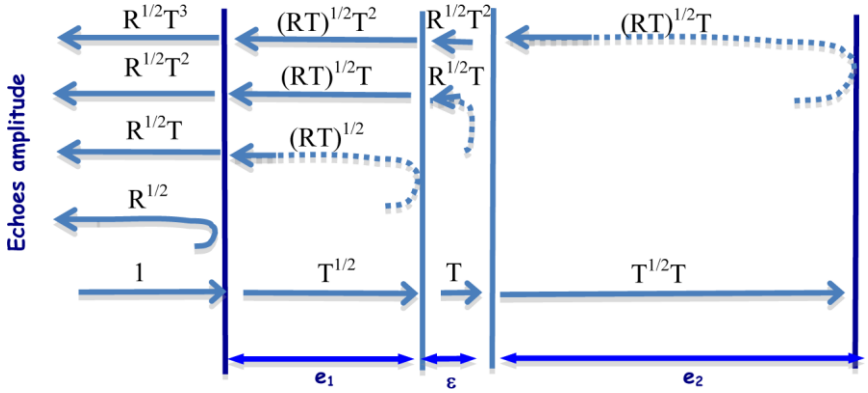

Fig. 2. Model interfaces and amplitudes of the light echoes. T and R: transmission and reflection intensity coefficients for each interface.

Assuming that the object (cornea) is constituted of only two slices (Fig. 2) of same index n and of thickness e_1 and e_2, separated by a very small air gap ε ($\varepsilon \approx 0$), the amplitude distributions S_R and S_T in the reference and object arms in front of each grating are then given by Eq. (1) [27]:

$$S_R(r,\nu) = \alpha_R S_s(r)\Gamma(\nu)\exp\left(-j\frac{2\pi\nu}{c}l_R\right)$$

$$S_T(r,\nu) = \alpha_T S_s(r)\Gamma(\nu)\sqrt{R}\exp\left(-j\frac{2\pi\nu}{c}l_T\right)\left[1+T(1+T)\exp\left(-j\frac{4\pi\nu n e_1}{c}\right)+T^3\exp\left(-j\frac{4\pi\nu n(e_1+e_2)}{c}\right)\right] \quad (1)$$

$S_s(r)$ and $\Gamma(\nu)=\Gamma_0$ are respectively transverse amplitude distribution (first order Bessel function depending on the radial component $r^2 = x^2 + y^2$) and spectrum (constant function

#135460 - $15.00 USD Received 21 Sep 2010; revised 10 Nov 2010; accepted 12 Nov 2010; published 19 Nov 2010

depending on the optical frequency ν) of the light source. The coefficients α_R and α_T correspond to the reflected and transmitted waves amplitudes by the different beam-splitters. R and T are respectively the reflection and the transmission intensity coefficients (T = 1-R) of each interface. l_R and l_T are the total paths in air for each arm of the interferometer.

These waves S_R and S_T are phase shifted by the two gratings of the SISAM that plays the role of correlator between the object and reference fields. The resulting wave, on the whole frequency bandwidth $\Delta\nu$ of the optical system, yields to the direct temporal intercorrelation signal $E_c(X)$ on the detector:

$$E_c(X) = E_0 + E_1(X)\sin c\left(\pi\Delta\nu\left(\frac{\Delta l}{c}+QX\right)\right) + E_2(X)\sin c\left(\pi\Delta\nu\left(\frac{\Delta l+2ne_1}{c}+QX\right)\right) + E_3(X)\sin c\left(\pi\Delta\nu\left(\frac{\Delta l+2n(e_1+e_2)}{c}+QX\right)\right) \quad (2)$$

where: E_0 = constant factor,

$$E_1(X) = 2S_S^2\Gamma_0^2\alpha_R\alpha_T\sqrt{R}\cos\left(\frac{4\pi\nu_0}{c}X\sin\left(\theta'_p-\theta'_0\right)+2\pi\nu_0\frac{\Delta l}{c}\right),$$

$$E_2(X) = 2S_S^2\Gamma_0^2\alpha_R\alpha_T\sqrt{R}T(1+T)\cos\left(\frac{4\pi\nu_0}{c}X\sin\left(\theta'_p-\theta'_0\right)+2\pi\nu_0\frac{\Delta l+2ne_1}{c}\right),$$

$$E_3(X) = 2S_S^2\Gamma_0^2\alpha_R\alpha_T\sqrt{R}T^3\cos\left(\frac{4\pi\nu_0}{c}X\sin\left(\theta'_p-\theta'_0\right)+2\pi\nu_0\frac{\Delta l+2n(e_1+e_2)}{c}\right)$$

$\Delta l = l_T - l_R$ is the difference of the reference and object optical paths in air. X is the horizontal coordinate perpendicular to the grating lines (Fig. 1) in the detector plane and $Q = 2\left[-\frac{N_0}{\nu_0\cos\theta'_0}\cos\left(\theta'_p-\theta'_0\right)+\frac{1}{c}\sin\left(\theta'_p-\theta'_0\right)\right]$ is the SISAM scale factor.

N_0 is the grating lines number per millimeter, θ'_0 the diffraction angle for the source central frequency ν_0 and θ'_p the diffraction angle corresponding to the optical frequency ν_p for which the flat tint is achieved (beams are superposed). The mathematical definition of X and calculation steps to obtain Q have been already developed [29].

Equation (2) exhibits 4 terms: a continuous background E_0 and three vertical correlation peaks of full width $\Delta X = \frac{2}{\Delta\nu Q}$ centered at $X_0 = -\frac{\Delta l}{cQ}$, $X_1 = -\frac{\Delta l+2ne_1}{cQ}$ and $X_2 = -\frac{\Delta l+2n(e_1+e_2)}{cQ}$.

The three peaks are spatially modulated at $\frac{2\nu_0}{c}\sin\left(\theta'_p-\theta'_0\right)$ frequency, are centered at the position corresponding to group delays of each of the reflected waves by the cornea and are weighted by the SISAM scale factor Q.

3. Calibration and numerical processing of the correlation signal

3.1 Calibration

At first, to calibrate the set-up, a mirror is used as object and set at the focal plane of the microscope objective. Inside its spatial envelope, the signal captured by the video camera exhibits, in this case, only one vertical correlation peak due to the single echo reflected by the mirror [27]. For each position LR_i of the delay line, the 2D-CCD camera shows the correlation signal including the vertical correlation peak that stands at different areas in the image. As

#135460 - $15.00 USD Received 21 Sep 2010; revised 10 Nov 2010; accepted 12 Nov 2010; published 19 Nov 2010

explained in the following paragraph (*§3.2 Numerical processing*), the peak is localized (pixel number) using a program developed with Matlab. The relationship between the pixel number (corresponding to the peak position) and the delay line position (corresponding to the object position) leads to a conversion coefficient of 1.023 µm/pixel.

With the help of Eq. (2) and knowing the opto-geometric characteristics of the set-up ($\Delta\lambda$ = 600 nm, λ_0 = 700 nm, $\theta'_0 = \theta'_p$ = 62.4° and N_0 = 150 l/mm), this conversion coefficient is first used to calculate theoretical peak full width leading to a theoretical axial resolution of 0. 8 µm (0,78 pixel). This is much smaller than the measured width value of 12 pixels leading to an axial resolution of 6 µm. This discrepancy could be explained by the fact that, even if dispersion brought by the microscope objective has been compensated, there is still residual phase distortion induced by the gratings that has not been taken into account in the calculus. This proves that the axial resolution is not limited by the spectral sensitivity of the CCD but by the dispersion of the set-up. Despite of the broadening of the correlation peak, the performance of the set-up in terms of axial resolution have been increased compared to [27] (6 µm instead of 40 µm).

Using one of these calibration measurements corresponding to the correlation peak standing roughly at pixel position X = 600 (central part of the signal), sensitivity could also be experimentally estimated. After numerical processing, the maximum peak amplitude (maximum inside the signal envelope) and the standard deviation expressed in grey level sum are 12900 and 250 leading to Signal to Noise Ratio equals to SNR = 18 dB. Even if the sensitivity of our method seems very similar to that of TD-OCT, it is not exactly the same. The OCT with shot-noise limited detection system considers mainly the properties of the detector and of the incoming light onto the sample [30]. In our case, the sensitivity also depends on the position X of the correlation signal and then on the considered depth value. This is due to the spatial envelope of the signal that is not constant along the X-axis: the sensitivity is then better in the central part of the correlation signal (it means at half the depth measurement range).

After this calibration, the mirror could be now removed and the different rabbit corneas set in place in order to be tested.

3.2 Numerical processing

We have used the well-known shift-and-add method to process the images delivered by our video camera. The images are first spatially translated so that the images motions due to very small corneas movements caused by slight corneal dehydration are removed. The very weak corneal thinning associated to dehydration is then averaged by the numerical process and has not been studied in the frame of this work. Afterwards, the images are added, leading to a gain for the signal to noise ratio equal to the square root of the number of processed images. In our case, all images have the same quality and so image selection is not necessary. Even if this method is already of current use in astronomy community, its use combined with the numerical process explained below is innovative for corneas interfaces detection.

For one particular cornea, an example of the resulting correlation signal (1280*960 pixels) when adding 20 images is shown in Fig. 3. Along the vertical coordinate y, the spatial intensity distribution of the probe beam stands in grey level. Actually, the set-up does not realize an image of the cornea in the y direction because the focusing objective permits to examine only the central part of the cornea. Indeed, the lens L_2 does not image the whole cornea but the central line of the gratings along the y direction on the CCD. The probing light is then incident on the sample along one direction (optical axis z) in a similar way as for one A-Scan. The correlation signal is obtained only if the probe beam is centered on the cornea otherwise the light reflected by each interface does not go back through the microscope objective because of the curvature of the cornea. Once centered on the cornea, the horizontal coordinate X gives immediately the correlation signal $E_c(X)$ [Eq. (2)] and then depth information about each interface. The peaks due to the two extreme interfaces are clearly visible along the vertical y direction.

#135460 - $15.00 USD Received 21 Sep 2010; revised 10 Nov 2010; accepted 12 Nov 2010; published 19 Nov 2010

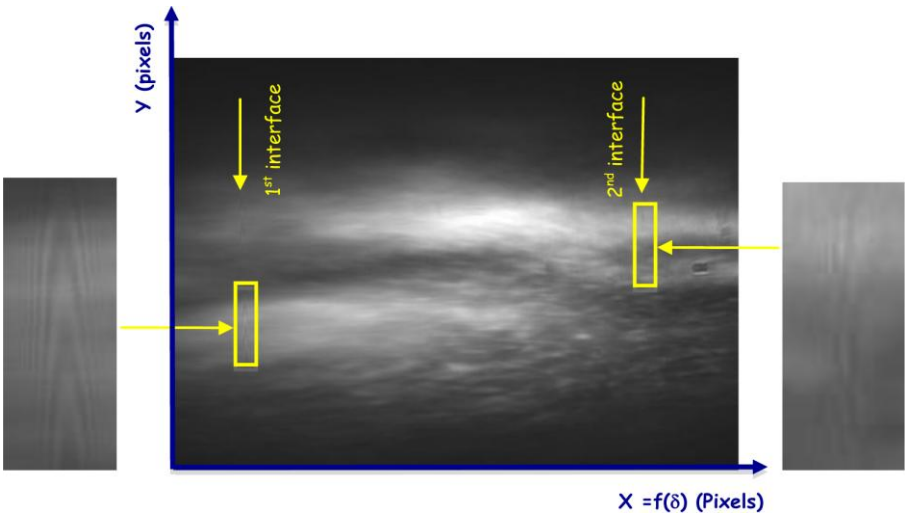

Fig. 3. Correlation signal.

Then, the numerical processing developed with Matlab and previously published [27] is applied to the signal. The signals corresponding to the object and reference arms are subtracted from the raw correlation signal of Fig. 3 in order to suppress the continuous background (due to light source spatial envelope). A region of interest (1238*400 pixels) of this pre-processed signal is then selected and a vertical Prewitt filter (method for edge detection) is applied to this region for extraction of the strong contrast areas. The two vertical correlation peaks corresponding to the extreme interfaces are visible in Fig. 4. The first one seems to be split into two peaks but corresponds to the same interface. This is due to fringes modulation inside the peak envelope (see §2.2). The peak corresponding to the second interface undergoes also such a modulation that is less visible. Another weak vertical peak stands around pixel 400. This will be confirmed in the following experimental results (§4).

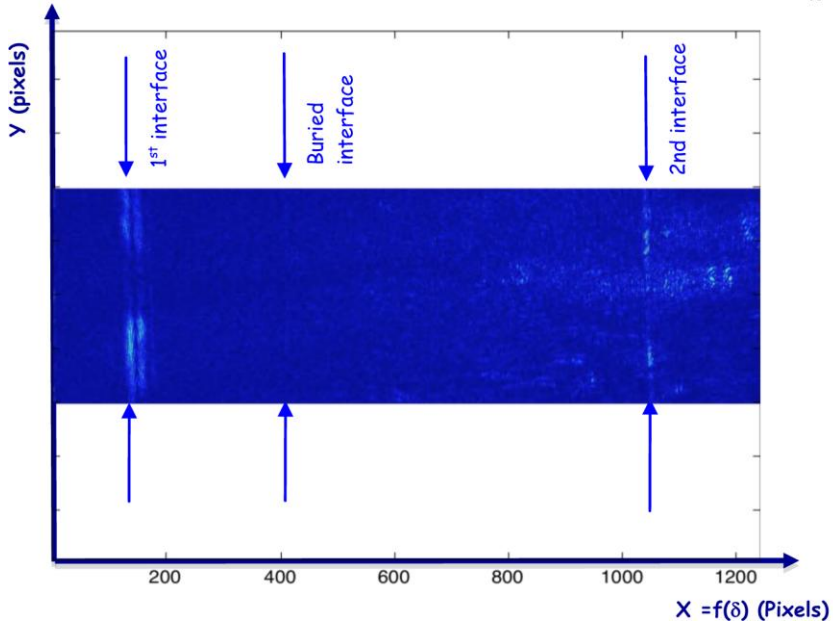

Fig. 4. Prewitt filter applied to the signal of Fig. 3.

#135460 - $15.00 USD Received 21 Sep 2010; revised 10 Nov 2010; accepted 12 Nov 2010; published 19 Nov 2010

The final correlation signal is obtained by summing the grey levels of the 400 lines on each column of the region of interest. This permits to enhance the signal and justifies the use of a 2D-CCD array instead of a line–scan camera. Then, each peak is automatically detected by search of the maxima inside the signal: all the values exceeding a given threshold are taken into account. For each X pixel, the threshold is chosen as the local mean value increased by three times the standard deviation calculated for 250 pixels around the considered X pixel. Consequently, this threshold value varies for each X position and takes into account the neighboring points. So, the choice of this numerical processing to detect the correlation peaks is justified by the fact that the sensitivity is a function of X position. Furthermore, when two peaks are too closed from each other, the weaker is automatically rejected; that is why in Figs. 5 and 6, only the first part of the double peaks corresponding to the first interface is detected. Few numerical values of thresholds and peak amplitudes are given in the experimental results (§4).

4. Experimental results

Two series of measurements were performed on rabbit corneas. All procedures conformed to the ARVO Statement for the Use of Animals in Ophthalmic and Vision Research.

4.1 Cornea with post-mortem surgery

Eyeballs were retrieved on rabbits obtained from a local slaughterhouse within 6 hours after death. Corneas were dissected with a scleral rim and immediately fixed in 4% paraformaldehyde, a crosslinking fixative, in order to maintain its normal shape and transparency. Cornea was maintained on an artificial chamber (Baron, Ioltech, France) and the intrastromal dissection, mimicking the LASIK flap creation was performed under an operating microscope using a crescent knife. The flap was created at the junction of the first anterior third (100µm $<e_1<$ 180µm) and the posterior two thirds (300µm $<e_1 + e_2<$ 500µm).

The cornea is removed from the preservation medium and immediately set in air at the sample place. The correlation image recorded by the detector is shown in Fig. 3. After subtraction of the background and the numerical processing explained in §3.2, three correlations peaks appear in the correlation signal (Fig. 5: red squares correspond to detected peaks) confirming the detection of three interfaces and particularly the interface corresponding to the flap.

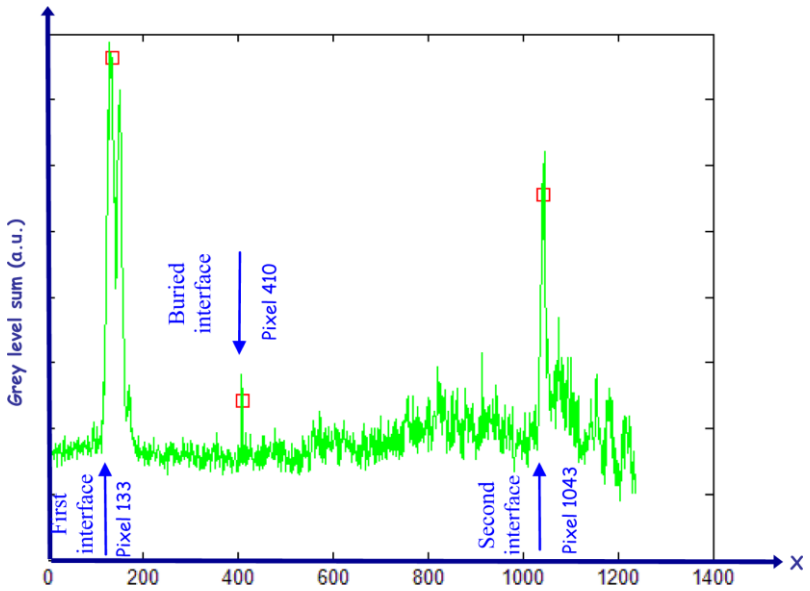

Fig. 5. Signal obtained after ex vivo flap dissection on a rabbit cornea.

#135460 - $15.00 USD Received 21 Sep 2010; revised 10 Nov 2010; accepted 12 Nov 2010; published 19 Nov 2010

Even if the buried interface is not visible in Fig. 3 and hardly distinguished in Fig. 4, the correlation peak is easily detected when applying the whole numerical process to the signal. In Fig. 5, the different peaks induced by each interface of the cornea are localized at pixels positions $X_0 = 133$, $X_1 = 410$ and $X_2 = 1043$. The optical paths differences $\delta_1 = ne_1$ and $\delta_2 = ne_2$ are corresponding to 247 and 633 pixels leading to a total cornea central thickness of $e_1 + e_2 = 675 \pm 4$ µm with a buried interface at $e_1 = 205 \pm 4$ µm from the anterior face and at $e_2 = 470 \pm 4$ µm from the posterior face (the cornea refractive index is $n = 1.38$ and the conversion coefficient of 1.023 µm/pixel §3.1). These experimental values agree with the flap dissection: the flap is realized at 1/3 from the first interface ($e_1 / (e_1 + e_2) = 0.3 \# 1/3$).

The uncertainty of 4 µm has been explained in the reference [27]. It has been estimated from a set of five correlations' signals recorded with the same experimental conditions and each correlation peak is localized at worst at one pixel position around ± 2 pixels (corresponding to 4 µm). The uncertainty depends only on the Signal to Noise Ratio and then on the sensitivity of the set-up and the ability of the software to localize one correlation peak. It does not depend on the peak width that limits only the resolution. As the buried interface peak is not localized at the edges of the signal, it is easier to detect it because of the higher sensitivity at the central part of the signal.

It has to be noticed that other peaks due to noise are located at different pixel positions but they are not detected by our software as for example the pixel X = 914. As a matter of fact, even if the amplitude ($y_X = 568$) of this peak seems high, it is yet less than the threshold value ($y_{thX} = 935$) calculated at this point by our processing (§3.2). The criterion chosen to calculate the threshold values is very efficient to discriminate signal from noise. Actually, the buried interface located at the pixel $X_1 = 410$ is perfectly detected whereas the peak amplitude ($y_1 = 216$) seems not very important, however it is higher than the threshold one ($y_{th1} = 204$).

The peak amplitudes ($y_0 = 2814$, $y_1 = 216$, $y_2 = 1782$) of all three detected interfaces are bound to their reflectivity, but could not be compared together because of the change of the sensitivity in function of the position X of the signal.

The value of the peak amplitude obtained for the buried interface is low but might be higher in case of LASIK eye. Actually, corneal tissue has not been ablated in our case whereas after LASIK surgery, an irregular layer of collagen appears at the ablated side of the interface. This corneal structure change modifies birefringence at buried interface and might be of benefit to give an increased correlation signal.

4.2 Cornea with surgery on living rabbit

In order to study the ability to detect interface after wound healing, mimicking the physiological conditions, a living new-Zealand white rabbit was operated under general anaesthesia with intra muscular ketamine and xylalazine. Topical anaesthesia with 0,4% oxybuprocaine chlorhydrate was used too. The central corneal thickness was determined with an ultrasonic pachymeter (SP-1000, Tomey, Tokyo, Japan) and a flap of approximately 8 to 9,5 mm of diameter was dissected at 120 µm of depth using an automated disposable microkeratome (One-Use-Plus, Moria, Antony, France) associated with an evolution 3E console. Postoperative treatment consisted of local instillation of antibiotics and steroids twice daily during the first two weeks. The animal was euthanized one month after surgery by lethal injection of Phenobarbital. Corneas were observed with a slit lamp and were clear. Interface was hardly visible. Both corneas were retrieved using the protocol previously described and immediately fixed in 4% paraformaldehyde. The cornea has been maintained in this preservation medium until being tested by our set-up.

Figure 6 gives the results for the correlation signal. The correlation peaks induced by each interface are localized at pixels positions: $X_0 = 62$, $X_1 = 407$ and $X_2 = 817$ leading to the central flap thickness $e_1 = 256 \pm 4$ µm and a total cornea thickness $e_1 + e_2 = 560 \pm 4$ µm.

#135460 - $15.00 USD Received 21 Sep 2010; revised 10 Nov 2010; accepted 12 Nov 2010; published 19 Nov 2010

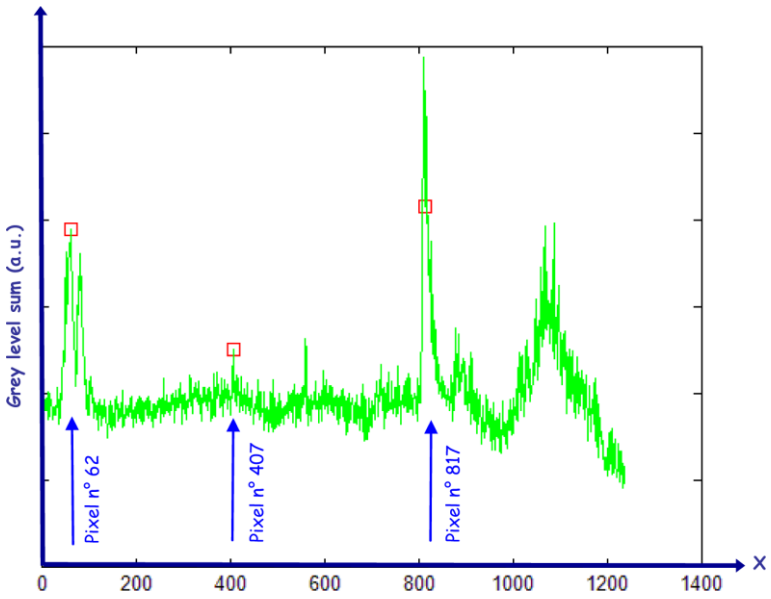

Fig. 6. Signal obtained after in vivo LASIK on a rabbit eye, followed by a 1-month wound healing (red squares corresponds to detected peaks).

The obtained results show that the peak corresponding to the flap is weak but it is detected when columns sum is realized (Fig. 6). Contrary to the first studied cornea, the reflectivity due to the surgery is here not very high, probably because of the healing process. When comparing the experimental thickness values with the ones obtained with the ultrasound pachymeter, the results are coherent. Indeed, the flap thickness just after surgery is measured by ultrasound to be roughly e_{1us} = 173 µm and the total cornea thickness e_{1us} + e_{2us} = 445 µm. After conservation in PFA solution, the cornea swells but the thickness ratio of the total cornea and the flap (e_1 + e_2)/ e_1 is nearly the same for ultrasound and low coherence interferometry measurements.

It must be noted that our software does not detect the peak located at pixel position 570. Even if the amplitude of this peak seems high, it is yet less than the threshold value calculated at this point by our processing (§3.2). Therefore, this peak due to noise is not taken into account. On the other hand, the buried interface located at the pixel X_1 = 407 is perfectly detected because its peak amplitude is higher than the threshold related to this pixel.

5. Conclusion

The initial set-up dedicated to contact lens thickness measurement [27] provides a fast correlation in real time with great accuracy and has been improved here for the detection of an interface in corneal anterior stroma. The changes applied for the measurement of the corneas are of three orders: the dispersion induced by the objective has been compensated in the set-up, the digital camera brings a better sensitivity and finally the numerical processing is innovative here as the fringes are readjusted before averaging several frames of the correlation signal. All these changes induce a better detection of weak amplitude signals compared to the one obtained with the initial set-up. Consequently, in this work, the ability to detect, in a single acquisition, the flap interface of a cornea has been demonstrated.

Despite the low speed of our detector (15 fps) compared to other 2D CCD (200 fps [18]) or CMOS cameras (3000 fps [31]), this method allows a single A-scan acquisition in 0,066 s. Full information about previous refractive surgery is contained in this single acquisition and the sum over 20 images permits only the enhancement of the Signal to Noise Ratio and consequently the sensitivity. Our method does not need any scan contrary to classical OCT.

#135460 - $15.00 USD Received 21 Sep 2010; revised 10 Nov 2010; accepted 12 Nov 2010; published 19 Nov 2010

Yet, OCT is able to perform 3D imaging of the entire cornea with several A-scans in few seconds and could bring complementary information about collagen structure.

Two corneas after surgery have been used as samples. The fringes contrast remains low because of the light scattering in rabbit corneas, even after PFA fixation. Nevertheless, even in these conditions, interfaces could be detected. Corneas stored in organ culture present a reversible stromal edema that will probably be responsible to a low fringes contrast but in the other hand the interface is likely to be enhanced by the swelling of the interface wound, described as the interface fluid syndrome [32]. The ability of our device to detect LASIK interface in human will be assessed on human cornea after dissection of a flap followed by several weeks of organ culture to allow a wound healing. This further application to human cornea using tissues devoted to scientific use thanks to body donation to Science, is the next logical step before possible translation to the routine in eye banks.

#135460 - $15.00 USD Received 21 Sep 2010; revised 10 Nov 2010; accepted 12 Nov 2010; published 19 Nov 2010